Kummerow, J., Raab, S. (2015): Temperature Dependence of Electrical Resistivity – Part II: A New Experimental Set-up to Study Fluid-saturated Rocks. - *Energy Procedia*, *76*, p. 247-255.

DOI: http://doi.org/10.1016/j.egypro.2015.07.855

Available online at www.sciencedirect.com

ScienceDirect

Energy Procedia 76 (2015) 247 – 255

Energy Procedia

European Geosciences Union General Assembly 2015, EGU

Division Energy, Resources & the Environment, ERE

Temperature dependence of electrical resistivity - Part II: A new experimental set-up to study fluid-saturated rocks

Juliane Kummerow[a,*], Siegfried Raab[a]

[a]*GFZ German Research Centre for Geosciences, Telegrafenberg, 14473 Potsdam, Germany*

Abstract

The growing interest in exploiting supercritical geothermal reservoirs calls for the understanding of the physical properties of rocks and the fluids they are interacting with in a high enthalpy environment. Here, we present a new flow-through cell capable for petrophysical measurements of fluid saturated rocks at high pressure and temperature. The permeability and electrical resistivity of a quartz-gabbro from a fossil hydrothermal system on Iceland were determined between 25 – 350 °C at a controlled pore pressure of 22.2 MPa. The measured resistivities are correlated with fluid resistivity data obtained in an attendant study (see part I of this paper).

Peer-review under responsibility of the GFZ German Research Centre for Geosciences

Keywords: high-temperature geothermal systems; fluid-rock interaction; electrical resistivity of rocks; permeability

1. Introduction

There is a growing scientific and economic interest in the exploration and exploitation of supercritical geothermal reservoirs to increase the efficiency of geothermal power plants [1,2]. The utilisation of geothermal energy requires, in any case, the detailed knowledge of the reservoir. In reservoir engineering, the characterisation of a geothermal system by electrical resistivity tomography (ERT) is a common geophysical exploration and monitoring strategy. However, for a realistic interpretation of the field measurements it is necessary to know both the physical properties of the rock and those of the interacting fluid at defined temperature and pressure conditions. While there have been made great effort in determination of physical and chemical properties of water above its critical point ($T_{critical}$ = 374.21 °C and $p_{critical}$ = 22.12 MPa), the influence of fluid-rock interactions on petrophysical properties in a high temperature environment is scarcely known. The technical complexity of high-temperature applications of experimental set-ups for the measurement of physical rock parameters at controlled pore pressure is very high and limits the available data. Duba et al. [3] and Milsch et al. [4] studied the electrical resistivity of metashales and volcanic rocks in flow-through experiments up to 150 °C. Kuhlenkampff et al. [5] and Llera et al. [6] have investigated sandstones and volcanic rocks in the range of 25 – 250 °C. For near-critical and supercritical conditions, both the experimental

* Corresponding author. Tel.: +49-331-288-1446 ; fax: +49-331-288-1450.
E-mail address: juliane.kummerow@gfz-potsdam.de

Peer-review under responsibility of the GFZ German Research Centre for Geosciences
doi:10.1016/j.egypro.2015.07.855

database as well as theoretical assumptions become weak. Ucok et al. [7] have reported on resistivity measurements up to 350 °C; Fuji-ta et al. [8] extended the temperature range up to about 830 °C to study the electrical response on dehydrating amphibolites, and Glover et al. [9] have introduced an advanced experimental design for electrical conductivity measurements at temperatures up to 900 °C and up to 1 GPa confining and pore pressure. However, all three high-temperature set-ups do not offer the possibility of fluid flow and pore pressure control.

Generally, the electrical conductivity of fluid saturated rocks results from the interconnected porosity, the conductivity of the free pore fluid, and the surface conductance of the rock-forming minerals. In a first approximation free fluid and interlayer conductivity are acting electrically in parallel [10]. The electrolytic conduction in pore fluids is related to chemical parameters of the solution, like the concentration of free charge carriers and ion species, and structural parameters of the porous medium such as porosity and the connectivity of the pore system [e.g.11]. Surface conductance results from electrochemical interactions between water dipols or ions and negatively charged mineral surfaces. Its contribution to the overall sample conductivity depends on the surface charge density, i.e. the mineral and fluid composition, as well as the specific internal surface area [5]. All these parameters are influenced by pressure, temperature, and electrolyte concentration [7]. From batch experiments it is obvious that the fluid composition can alter significantly in dependence of permeability, pressure, temperature, and mineral composition of the porous medium [12,13] and thus the concentration of charge carriers will change. At supercritical conditions the viscosity of the fluid is low, which enhances the mass transfer and diffusion-controlled chemical reactions. This may have considerable effects on the physical properties of both the fluid (fluid resistivity) and the rock (porosity, hydraulic properties).

However, the fundamental understanding of the impact of hydrothermal alteration on the pore structure of a rock and the fluid composition and thus, the electrical behaviour of geothermal systems at near- and supercritical conditions is still required. For a better understanding of fluid-driven processes in geological settings with a high heat flow the investigation of fluid-rock interactions is crucial. To investigate high-enthalpy fluid-rock systems, in the framework of the current, EU-funded FP7-project IMAGE (Integrated Methods for Advanced Geothermal Exploration) we have developed a new flow-through system to measure the electrical resistivity and permeability of rock samples up to supercritical conditions of aqueous fluids (pore pressure = 40 MPa, temperature = 400 °C). So far, we have successfully tested the system up to 350 °C. Here, the experimental set-up and first results obtained with the new measuring cell are presented. The obtained data are correlated to temperature-dependent resistivities of the used pore fluid, which were determined in a second high-temperature measuring cell introduced in the first part of this paper. It is far beyond the scope of this paper to give a final interpretation of the measured physical properties. Primarily, this paper serves to demonstrate the feasibility of high temperature resistivity and permeability measurements and to depict the experimental limits.

2. Experimental set-up

Besides the experiments with fluids, which were described in part I of this paper, petrophysical measurements are performed with brine percolating through a rock sample at controlled pore pressure. To measure the electrical resistivity and the permeability of rocks at high temperatures an internally heated argon gas pressure chamber with five non-interrupted thermocouple lines for a precise temperature control and feed throughs for electrical conductivity measurement was upgraded by a pore fluid pressure system. The vessel can be operated at pressures up to 60 MPa at temperatures of up to 400 °C. The pore fluid system is controlled by two pumps. At up-stream side a HPLC pump injects synthetic formation brine into the sample, while a syringe pump at the down-stream side adjusts the pore pressure (Fig. 1a). In detail, the measuring cell consists of a hollow cylindrical rock sample, which is 30 mm in diameter and 75 mm in length (Fig. 1b). The core is placed between two ceramic buffer rods and jacketed with a chemically inert gold tube. The ends of the gold tube are sealed pressure-tight to the buffers with a temperature stable epoxy resin. For resistivity measurements a second gold tube is installed in the central borehole. To heat up the sample we use a 2-zone furnace, where both zones are independently controlled via thermocouples in direct contact to the heater elements. Two additional thermocouples in the center axis of the sample, and located near its ends, control the sample temperature. In both ceramic buffers fluid ports are glued to connect the 1/16” fluid capillaries (Hastelloy). The inlet capillary is coiled around the furnace to preheat the fluid during its passage. In contrast, the ends of the ceramic buffers are cooled with blocks of massive aluminium to prevent the glue-sealings from over-heating. So far, the measuring cell was calibrated and successfully tested up to 40 MPa confining pressure, 22.2 MPa pore pressure

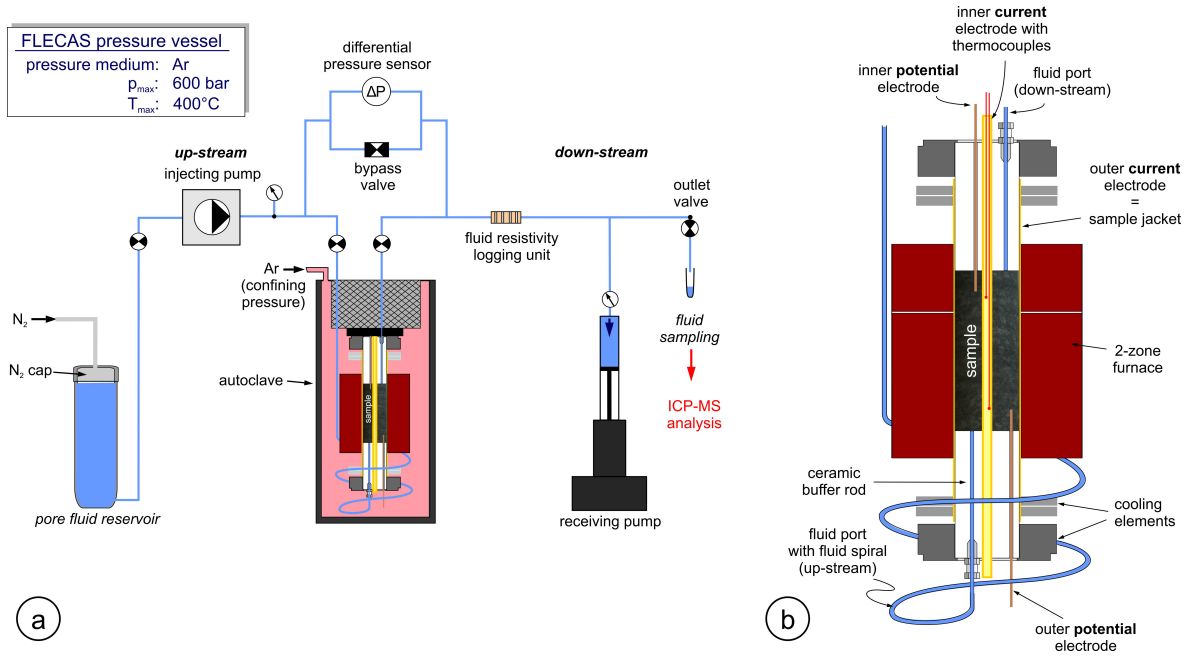

Fig. 1. (a) Schematic overview of the experimental device; (b) Close-up of the sample measuring cell.

and 350 °C. However, supercritical conditions have not been applied yet, as at temperature of 350 °C leakage of the fluid system occurred, most probably because of overheating a glue sealing. Currently, we adjust the construction for optimising the cooling of the buffers to extend the temperature range up to supercritical conditions (> 375 °C).

3. Measuring procedure

A dry sample is placed in the measuring cell and sealed in the autoclave. Then, a low confining pressure (p_{conf} = 6.5 MPa) is applied. For sample saturation the total system including test core, capillaries, valves and pressure sensors is evacuated. At a pressure of 20 Pa the system is flooded with the synthetic pore fluid delivered by the brine pump at a low injection rate (Q = 0.05 ml/min). Concurrently, the electrical resistivity is monitored. We assume full sample saturation, when the resistivity reaches constant values. Then the flow is stopped, the set-up is connected to the down-stream pump, and both the confining and the pore pressure are incrementally increased up to the pressures aspired during the experiment (p_{conf} = 26 MPa, p_{pore} = 22.2 MPa). The sample is allowed to equilibrate to experimental conditions for about 24 h before the experiment is started at isobaric conditions for increasing temperatures. At each temperature step the electrical and hydraulic conductivity of the sample are measured. The experiment is run as a discontinuous flow through experiment. That means, the fluid flow is stopped before the new temperature is set, to avoid a mixing of fluids that were exposed to the sample at different temperatures. After the sample is led to equilibrate to the new temperature, the resistivity is measured for static conditions (without fluid flow). Before the flow is started again, fluid samples have been taken down-stream for further analyses. For this, the receiving pump has been drained down to 4 ml, the volume that is required to return to pore pressure level, before the valve between measuring cell and pump was opened again and the flow was re-started. For permeability measurements a certain flow rate is adjusted and kept constant for several hours until the differential pressure reached equilibrium.

3.1. Determination of electrical resistivity

Rock resistivities are determined as function of temperature with the cell, which is schematically shown in Fig. 1b. We use a four-electrode layout in a coaxial arrangement to avoid effects of contact resistance between measuring

electrodes and sample. The current is supplied to the sample via the gold tubes, which generates a radial electrical field. The voltage is detected with two additional potential electrodes, that are placed in blind holes inside the rock sample. For resistivity measurements an impedance spectrometer (Zahner-Zennium electrochemical workstation) supplies an AC voltage with amplitude of 500 mV at different frequencies ranging from 10 mHz to 10 kHz. The Zahner-bridge measures impedance, Z, and phase angle, ϕ, at distinct frequencies. The sample resistance, R, is given by

$$R = cos\phi \cdot Z \tag{1}$$

The bulk resistivity of the sample, ρ_b, is calculated from sample resistance and the cell constant, c, which considers the geometry of the electrode layout

$$\rho_b = \frac{R}{c}. \tag{2}$$

ρ_b can also be expressed as conductivity, $\sigma_b = 1/\rho_b$.

For the calibration of the resistivity cell the volume reserved for the rock sample was filled one after the other with distilled water, tap water, and aqueous NaCl solutions of 0.1 and 1 molarity and the cell resistivity was measured. The cell constant is given by the slope of the plot of cell resistivity versus corresponding fluid resistivity, ρ_{fl}, which is measured as fluid conductivity, σ_{fl}, with a commercial fluid conductivity sensor. The cell constant, received from the calibration at ambient conditions, is used to calculate resistivities of rock samples at all temperatures applied during the experiment. Changes in the resistivity due to cooling effects during the percolation of the pore fluid were found to be about 0.1 % for a fluid percolation of 0.05 ml/min over 9 hours. The experimental error on sample resistivities due to variations in the set-up dimension at elevated pressure and temperature, cooling effects of the flown pore fluid, and instrumental accuracy cumulates to ± 2 %.

The set-up does not allow for the measurement of fluid resistivity at sample temperature. However, at each temperature step the conductivity of the fluids sampled at the outlet valve was measured with a commercial fluid conductivity sensor. Recently, we have built a fluid resistivity-logging unit for down-stream installation to monitor changes in the resistivity for a defined temperature and the applied pore pressure.

3.2. Determination of permeability

For the permeability measurement the sample is percolated with the pore fluid at flow rates ranging between 0.02 and 0.1 ml/min. However, it was found that the hydraulic equilibrium was highly disturbed by changes in the flow rates. Thus, preferentially we worked with a flow rate of 0.05 ml/min, which is kept constant for at least 9 h to ensure an equilibrated differential pressure. The differential pressure, Δp, which builds up between up-stream and down-stream side is measured with a differential pressure sensor in a range of 2 MPa (resolution = 0.01 MPa). The permeability is calculated after Darcys law, considering the given flow rate, Q, the fluid viscosity at experimental conditions, $\eta_{(T,p_{pore})}$, the measured differential pressure Δp, and the known sample geometry, G:

$$k_{(p,T)} = \frac{Q \cdot \eta_{(T,p_{pore})}}{\Delta p} \cdot G, \tag{3}$$

with

$$G = \frac{l_s}{A} = \frac{l_s}{\pi\left(r_s^2 - r_h^2\right)}, \tag{4}$$

where l_s is the length of the sample and A is the effective sample cross section, that is calculated from the sample radius, r_s, and the radius of the central hole, r_h. As fluctuations in flow rate are a severe error source in permeability determination the flow rate given by the injecting pump was crosschecked with the volume received at the down-stream pump for a defined time interval. Differences in the flow rate were lower than 1 %. Additionally, the flow rate through the sample was corrected for the temperature difference between pump and sample with the help of the

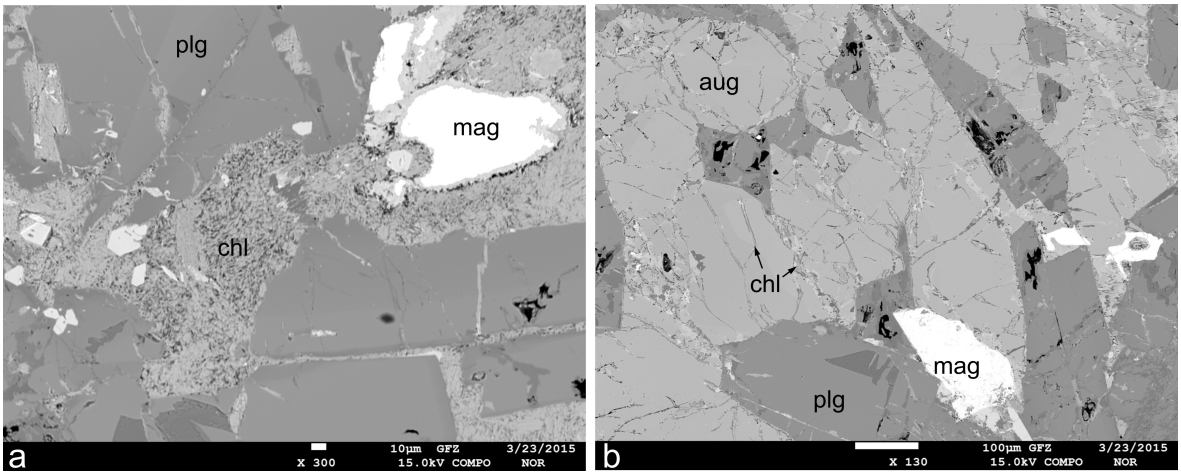

Fig. 2. SEM images of the sample material. Two types of porosity can be identified: an intrinsic porosity, which is associated with chlorite aggregates (a) and an artificial porosity linked to grain boundaries and re-opend fractures after thermal cracking (b). Cracks are often coated with chlorite minerals. aug: augite, chl: chlorite, mag: magnetite, plg: plagioclase.

temperature and pressure dependent molar volumes taken from the NIST webbook [14]. Due to a lack of viscosity data for salt solutions at higher temperatures, the fluid viscosity $\eta_{(T,p_{pore})}$ at the pore pressure and sample temperature was taken from NIST webbook as well, assuming that the viscosity of a 0.016 molal aqueous salt solution does not differ significantly from those of pure water. The overall error on permeability measurements is assumed to be within ± 2 %.

4. Sample material

In the framework of the FP7-project IMAGE, so far, resistivity and permeability measurements have been performed on a dense quartz-gabbro from a fossil, exhumed supercritical system located at Geitafell (S-Iceland), which serve as proxy for the recent Krafla hydrothermal reservoir (NE-Iceland). Based on SEM and XRD analyses the mineral composition of the gabbro comprises plagioclase (44 %), augite (24 %), hornblende (14 %), chlorite (13 %), magnetite (3 %), and quartz (2 %). The porosity of 1.2 % is predominantely associated to micropores in chlorite aggregates (Fig. 2a). At ambient conditions the sample is impermeable. However, from microscopic healed cracks it is evident that the sample was permeable once and fluid transport in the fossil reservoir was presumably fracture-dominated (Fig. 2b). To increase the permeability of the studied core, partially these chlorite coated cracks have been re-opened prior to the experiment by thermal cracking under an inert gas (Ar) atmosphere. This procedure increased the porosity to 6.2 % and the permeability to 1.28 mD at ambient conditions.

As pore fluid a synthetic brine of Krafla composition (15 mM/l NaCl, 0.721 mM/l $CaCl_2$, 0.643 mM/l K_2SO_4) was mixed from high-purity salts and distilled water on the basis of published fluid analyses [15]. The conductivity of the mixture is 0.206 S/m at ambient conditions. To reduce the corrosion risk of the experimental device (capillaries, fittings, valves, pumps), the fluid is sonicated and flushed for 24 h with nitrogen to expel O_2 from it and then pressurised with N_2 to avoid the re-dissolution of oxygen from air.

5. Preliminary results and discussion

The isobaric electrical resistivity and permeability of a quartz-gabbro from a fossil high enthalpy hydrothermal reservoir in Iceland were measured as function of temperature in a discontinuous flow through experiment. The results are plotted in Fig. 3.

Although the sample was thermally cracked prior to the experiment, it possesses a low permeability of 1.28 mD, which reduces by a factor of 10 to 113 μD for the applied effective pressure (Fig. 3a). Up to 200 °C the permeability

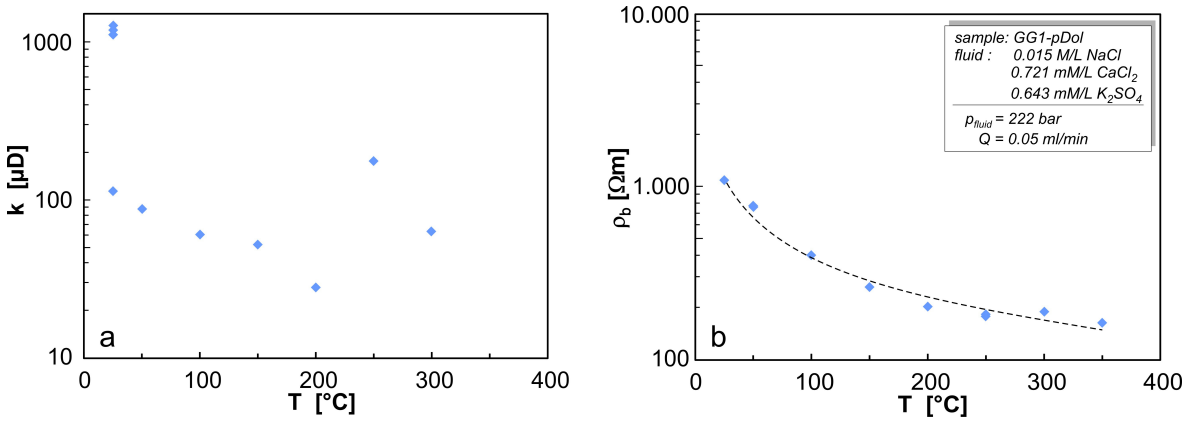

Fig. 3. Permeability (a) and electrical resistivity (b) of a quartz-gabbro from Geitafell/ Iceland measured as function of temperature. The reported resistivities correspond to a frequency of 100 Hz. Error bars are not shown, as the largest is of the size of the symbols.

decreases exponentially to 28 μD, what corresponds to a reduction in permeability of 75 %. However, at 250 °C the permeability suddenly increases to 170 μD. At this temperature we have applied various flow rates (0.02, 0.05, 0.07, 0.1 ml/min), which confirms the increase in permeability. Thus, we assume this value to be realistic. For 300 °C the permeability decreases again to an intermediate level. We have no data for 350 °C, because the hydraulic equilibrium was not achieved when the leakage occurred. Generally, it has been observed that the hydraulic equilibrium ($\Delta p_{(T=const)}$) becomes perturbed for hours by any changes in the flow rate, while constant rock resistivities have been attained already with the thermal equilibration of the sample.

In contrast to the permeability, the consolidation of the sample by raising the confining and pore pressure at room temperature has nearly no influence on the electrical resistivity of the rock sample as only a slight increase from $1.03 \cdot 10^3$ Ωm to $1.08 \cdot 10^3$ Ωm was observed. With increasing temperatures up to 350 °C the electrical resistivity decreases in a power law relationship (Fig. 3b) and shows thus a similar dependence on temperature as the saturation fluid (see part I of this paper).

The non-consistent behaviour of temperature dependence of permeability and resistivity indicates that the pore network contributing to the hydraulic and the electrical conductivity might not be identical. The fact that the permeability decreases for increasing pressure and at isobaric conditions with temperature, although the fluid flowing through it becomes less viscous, points to structural changes in that specific pore network. Two different porosities have been identified by analysis of thin-sections: a low intrinsic micro-porosity of 1.2 %, which is preferentially associated to aggregates of fine chlorite needles and an artificial porosity (additional 5 %) due to thermal cracking prior to the experiment, which is related to grain boundaries and the re-opening of pre-existing cracks. Shapiro [16] subdivide the total porosity of a rock into a compliant porosity supported by cracks and grain contact vicinities with an aspect ratio less than 0.01, where the aspect ratio denotes the ratio of the minimum and maximum axis of a pore [e.g.17], and a stiff porosity characterised by more or less isometric pores with aspect ratios typically larger than 0.1. Especially the compliant porosity can be largely affected by several factors, such as increasing pressure, temperature, and fluid-rock interactions. Thus, we assume that for the studied sample the permeability is related to a crack-dominated pore network and the stiff pores do not provide a significant contribution [18]. The mechanism leading to the decrease in crack porosity at constant pressure conditions is not fully understood, yet. One explanation might be the reduction of the effective pore aperture by thermal expansion of rock-forming minerals, until the thermal stress is high enough to develop new cracks or the precipitation of new minerals.

The network contributing to the electrical conductivity probably possesses higher aspect ratios, which alter only slightly with increasing pressure and temperature, while the degeneration of the compliant crack network seems not to affect the electrical properties of the rock. Generally, the current flow in a fluid saturated rock is mainly controlled by the electrolytic conduction of the pore fluid and by surface conduction at the interface between electrolyte and minerals [19,20]. At high fluid salinity (> 1 S/m), the current transport is dominated by fluid conduction, σ_{fl}, and

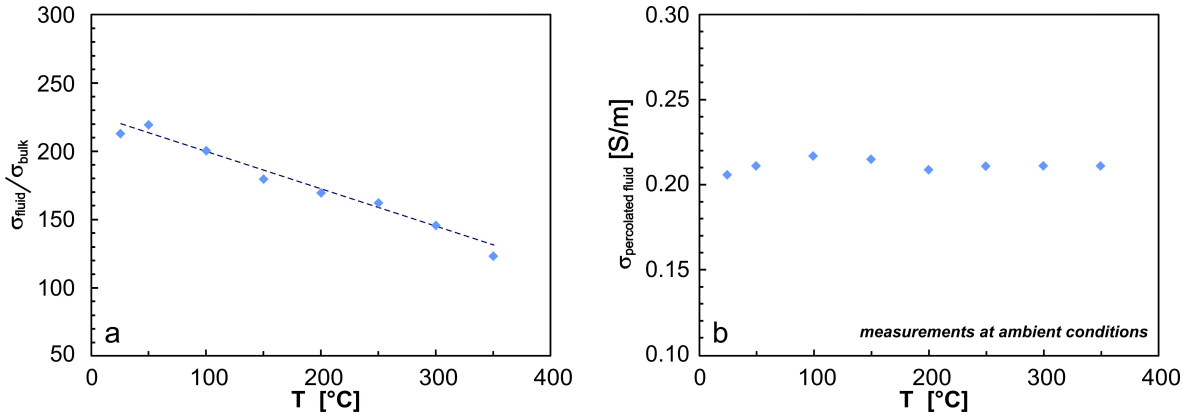

Fig. 4. (a) The ratio of σ_{fl}/σ_b vs. temperature; (b) Electrical conductivity of pore fluid exposed to various temperatures. Data are obtained for ambient pressure and temperature.

depends on the pore structure, which is represented by the formation factor, F, [e.g.11,21], that arise from Archie's relation [22]

$$\sigma_b = \frac{\sigma_{fl}}{F}. \tag{5}$$

For low fluid salinity (< 1 S/m) there has been described an increasing contribution of surface conduction, σ_s, to the bulk conductivity of the formation, σ_b, especially when clay-rich or low porosity rocks are involved [10]

$$\sigma_b = \frac{\sigma_{fl}}{F^*} + \sigma_s. \tag{6}$$

Surface conductance becomes the dominating mechanism for current flow in porous media saturated with highly diluted fluids of a fluid conductivity of < 0.2 S/m [11,19,20]. Hence, surface conductance is assumed to contribute significantly to the bulk conductivity of the studied sample. This is consistent with Fig. 4a, which shows the bulk conductivity of the rock normalised by the fluid conductivity at corresponding temperature. The linear decrease of the ratio indicates that the increase in sample conductivity with temperature is more pronounced than the observed conductivity increase of the Krafla fluid. Commonly, this exceeding conductance is attributed to electrochemical interactions at mineral surfaces [23]. Another mechanism, which has to be taken into account, is the effect of chemical fluid-rock interactions. During heating and thermal equilibration of the sample the pore fluid is exposed to the rock for about 10 hours, while during flow the residence time of the fluid is reduced to approximately 1 hour, defining a flow rate of 0.05 ml/min and an initial pore volume of 3.2 cm^3. To estimate the influence of fluid-rock interactions, fluid samples were taken at every temperature step for chemical analyses. However, so far the results are still outstanding. Additionally, the conductivity of the expelled pore fluid was measured at room temperature and atmospheric pressure (Fig. 4b). We found only a slight increase in conductivity from 0.206 S/m (prior to injection) to 0.212 S/m after the fluid was exposed to the rock sample. There were no hints for precipitations, as all filters and capillaries were still clean after the experiment. Nonetheless, it is assumed that the pore fluid is chemically influenced due to contact with the rock sample, as it is not in chemical equilibrium with the formation at the different temperature steps. The extent of fluid-rock interaction depends on pressure, temperature, mineral compositions, and the specific surface area. Due to the low permeability of the studied rock sample, the contact area between fluid and formation is limited and hence, the degree of fluid and rock alteration should be low in this study. This assumption is supported by the linear decrease in σ_{fl}/σ_b ratio (Fig. 4a). The release of ions from alterated minerals should increase the bulk conductivity of the sample, and hence, the ratio of σ_{fl}/σ_b should become lower, which at least is not visible in our data. However, for higher temperatures than the 350 °C applied so far, considerable fluid-rock interactions are expected.

6. Summary

This is a study under progress: We have built a new experimental set-up, which enables flow through experiments on rock samples under controlled confining and pore pressure at near critical temperature. So far, the system was tested for p_{conf} = 60 MPa and p_{pore} = 22.2 MPa at a preliminary maximum temperature of 350 °C. Electrical and hydraulic conductivity of a quartz-gabbro from a fossil geothermal reservoir in Iceland have been determined for increasing temperatures to better understand fluid-driven processes in geological settings with a high heat flow. The measured resistivity data were correlated with resistivities of the pore fluid, measured in an attendant study (part I). The experimental data show that fluid flow and current flow in our cracked sample prefer different pore networks, which act largely independent from each other. To complete the study, in the framework of the current project the petrophysical measurements will be supplemented by a number of additional tests: chemical analyses of fluid and rock samples before and after the experiment in combination with microstructural investigations of the original and percolated rock material will help to visualise microstructural changes and potential fluid-rock interactions. Experiments with different exposure times (flow rates) and/or different specific surface areas will allow deriving information about the dissolution kinetics and will help to model hydrothermal systems.

Acknowledgements

We wish to thank the machine shop of GFZ Potsdam and Mathias Kreplin for their support during the preparation of the experimental device. Many thanks are also due to Ronny Giese for his invaluable help during setting up the experiment. Sample material was kindly provided by Helga Margret Helgadottir, ISOR. We thank Rudolf Naumann for the kind introduction into XRD analysis, and Oona Appelt for her support at the microprobe. The manuscript was improved by many helpful discussions with Erik Spangenberg. This study is funded by the EU in the framework of FP 7-project IMAGE – "Integrated Methods for Advanced Geothermal Exploration" (grant agreement no. 608553).

References

[1] Albertsson A, Bjarnason JÖ, Gunnarsson T, Ballzus C, Ingason K. The Iceland Deep Drilling Project: Fluid handling, evaluation and utilization. International Geothermal Conference, Reykjavik, September 2003; 23-29.
[2] Fridleifsson GO, Elders WA. The Iceland Deep Drilling Project: a search for deep unconventional geothermal resources. Geothermics 2005; 34: 269-285.
[3] Duba A, Roberts J, Bonner B. Electrical properties of geothermal reservoir rocks as indicators of porosity distribution. Proceedings 1997, 22th Workshop on Geothermal Reservoir Engineering Stanford University, Stanford, California, January 27-29, 1997; SGP-TR-155.
[4] Milsch H, Kristinsdottir LH, Spangenberg E, Bruhn D, Flovenz OG. Effect of the water-steam phase transition on the electrical conductivity of porous rocks. Geothermics 2010; 39 (1): 106-114.
[5] Kuhlenkampff J, Spangenberg E, Flovenz O, Raab S, Huenges E. Petrophysical parameters of rocks saturated with liquid water at high temperature geothermal reservoir conditions. Proceedings, World Geothermal Congress 2005, Antalya, Turkey, 24-29 April 2005.
[6] Llera FJ, Sato M, Nakatsuka K, Yokoyama H. Temperature dependence of the electrical resistivity of water-saturated rocks. Geophysics 1990; 55: 576-585.
[7] Ucok H, Ershaghi I, Olhoeft GR. Electrical resistivity of geothermal brines. J Petrol Technol 1980; 32 (4): 717-727.
[8] Fuji-ta K, Katsura T, Ichiki M, Matsuzaki T, Kobayashi T. Variations in electrical conductivity of rocks above metamorphic conditions. Tectonophysics 2011; 504 (1-4): 116-121.
[9] Glover PW, Ross RG, Jolly H. The measurement of saturated rock electrical conductivity at lower crustal temperatures and high pressures. High Press Res 1990; 5: 705-707.
[10] Patnode HW, Wyllie MRJ. The presence of conductive solids in reservoir rocks as factor in electric log interpretation. Petrol Trans 1950; AIME 189: 47-52.
[11] Nover G. Electrical properties of crustal and mantle rocks a review of laboratory measurements and their explanation. Surv Geophys 2005; 26: 593-651.
[12] Browne PRL, Ellis AJ. The Ohaki-Broadlands hydrothermal area, New Zealand: mineralogy and related geochemistry. Am J Sci 1970; 269: 97-131.
[13] Ewers GR. Experimental hot water-rock interactions and their significance to natural hydrothermal systems in New Zealand. Geochem Cosmochem Acta 1971; 41: 143-150.
[14] Lemmon EW, McLinden MO, Friend DG. Thermophysical properties of fluid systems. In: Linstrom PJ, Mallard WG, editors. NIST Chemistry WebBook 2005; NIST standard reference database number 69; National Institute of Standards and Technology, Gaithersburg MD, 20899 (http://webbook.nist.gov).
[15] Arnórsson S, Axelsson G, Sæmundsson K. Geothermal systems in Iceland: Jökull. Icelandic J Earth Sci 2008; 58: 269-302.

[16] Shapiro SA. Elastic piezoensitivity of porous and fractured rocks. Geophysics 2003; 68 (2): 482-486.
[17] Zimmerman RW, Somerton WH, King MS. Compressibility of porous rocks. J Geophys Res 1986; 91: 12765-12777.
[18] Shapiro SA, Khizhniak GP, Plotnikov VV, Niemann R, Ilyushin PYu, Galkin SV. Permeability dependency on stiff and compliant porosities: a model and some experimental examples; J Geophys Eng 2015; 12 (3): 376-385; doi:10.1088/1742-2132/12/3/376.
[19] Waxman MH, Smits LJM. Electrical conductivities in oil-bearing shaly sands. J Soc Petrol Eng 1968; 8: 107-122.
[20] Revil A, Glover PWJ. Nature of surface electrical conductivity in natural sands, sandstones, and clay. Geophys. Res Lett 1998; 25 (5): 691-694.
[21] Einaudi F, Pezard PA, Ildefonse B, Glover P. Electrical properties of slow-spreading ridge gabbros from ODP hole 1105A, SW Indian Ridge. In:Havey PK, Brewer TS, Pezard PA, Petrov VA, editors. Petrophysical properties of crystalline rocks. Geol. Soc London Spec Pub 240; 2005.
[22] Archie GE. The electrical resistivity log as an aid in determining some reservoir characteristics. Petrol Trans 1942; AIME 146: 54-62.
[23] Ucok H. Temperature dependence of the electrical resistivity of aqueous salt solutions and solution saturated porous rocks. Ph.D. Dissertation, University of Southern California 1979; pp 164.